Suppressing lossy-film-induced angular mismatches between reflectance and transmittance extrema: optimum optical designs of interlayers and AR coating for maximum transmittance into active layers of CIGS solar cells

Yin-Jung Chang*

Department of Optics and Photonics
National Central University, Zhongli 32001, Taiwan
*yjchang@ncu.edu.tw

Abstract: The investigation of optimum optical designs of interlayers and antireflection (AR) coating for achieving maximum average transmittance (T_{ave}) into the $CuIn_{1-x}Ga_xSe_2$ (CIGS) absorber of a typical CIGS solar cell through the suppression of lossy-film-induced angular mismatches is described. Simulated-annealing algorithm incorporated with rigorous electromagnetic transmission-line network approach is applied with criteria of minimum average reflectance (R_{ave}) from the cell surface or maximum T_{ave} into the CIGS absorber. In the presence of one MgF_2 coating, difference in R_{ave} associated with optimum designs based upon the two distinct criteria is only 0.3% under broadband and nearly omnidirectional incidence; however, their corresponding T_{ave} values could be up to 14.34% apart. Significant T_{ave} improvements associated with the maximum-T_{ave}-based design are found mainly in the mid to longer wavelengths and are attributed to the largest suppression of lossy-film-induced angular mismatches over the entire CIGS absorption spectrum. Maximum-T_{ave}-based designs with a MgF_2 coating optimized under extreme deficiency of angular information is shown, as opposed to their minimum-R_{ave}-based counterparts, to be highly robust to omnidirectional incidence.

OCIS codes: (350.6050) Solar energy; (310.1210) Antireflection coatings; (310.4165) Multilayer design; (310.6860) Thin films, optical properties.

References and links

1. I. Repins, M. A. Contreras, B. Egaas, C. DeHart, J. Scharf, C. L. Perkins, B. To, and R. Noufi, "19.9%-efficient ZnO/CdS/CuInGaSe2 solar cell with 81.2% fill factor," Prog. Photovolt: Res. Appl. **16**, 235–239 (2008).
2. A. Chirilă, S. Buecheler, F. Pianezzi, P. Bloesch, C. Gretener, A. R. Uhl, C. Fella, L. Kranz, J. Perrenoud, S. Seyrling, R. Verma, S. Nishiwaki, Y. E. Romanyuk, G. Bilger, and A. N. Tiwari, "Highly efficient $Cu(In,Ga)Se_2$ solar cells grown on flexible polymer films," Nat. Mater. **10**, 857–861 (2011).
3. Y.-J. Lee, D. S. Ruby , D. W. Peters, B. B. McKenzie, and J. W. P. Hsu, "ZnO nanostructures as efficient antireflection layers in solar cells," Nano. Lett. **8**(5), 1501–1505 (2008).

#200659 - $15.00 USD Received 4 Nov 2013; revised 19 Dec 2013; accepted 25 Dec 2013; published 9 Jan 2014

4. J. W. Leem, Y. M. Song, and J. S. Yu, "Broadband wide-angle antireflection enhancement in AZO/Si shell/core subwavelength grating structures with hydrophobic surface for Si-based solar cells," Opt. Express **19**(S5), A1155–A1164 (2011).
5. P. Spinelli, M. A. Verschuuren, and A. Polman, "Broadband omnidirectional antireflection coating based on subwavelength surface Mie resonators," Nat. Commun. **3**, 692 (2012).
6. S. J. Oh, S. Chhajed, D. J. Poxson, J. Cho, E. F. Schubert, S. J. Tark, D. Kim, and J. K. Kim, "Enhanced broadband and omni-directional performance of polycrystalline Si solar cells by using discrete multilayer antireflection coatings," Opt. Express **21**(S1), A157–A166 (2013).
7. V. E. Ferry, M. A. Verschuuren, M. C. v. Lare, R. E. I. Schropp, H. A. Atwater, and A. Polman, "Optimized spatial correlations for broadband light trapping nanopatterns in high efficiency ultrathin film a-Si:H solar cells," Nano. Lett. **11**, 4239–4245 (2011).
8. B.-K. Shin, T.-I. Lee, J. Xiong, C. Hwang, G. Noh, J.-H. Cho, and J.-M. Myoung, "Bottom-up grown ZnO nanorods for an antireflective moth-eye structure on $CuInGaSe_2$ solar cells," Sol. Energy Mater. Sol. Cells **95**(9), 2650–2654 (2011).
9. Y.-J. Chang and Y.-T. Chen, "Broadband omnidirectional antireflection coatings for metal-backed solar cells optimized using simulated annealing algorithm incorporated with solar spectrum," Opt. Express **19**(24), A875–A887 (2011).
10. S. Hwang and J.-H. Jang, "3D simulations for the optimization of antireflection subwavelength structures in CIGS solar cells," in 38th IEEE Photovoltaic Specialists Conference (PVSC), pp. 000864–000867 (2012).
11. J. Mann, J. Li, I. Repins, K. Ramanathan, S. Glynn, C. DeHart, and R. Noufi, "Reflection optimization for alternative thin-film photovoltaics," IEEE J. Photovolt. **3**(1), 472–475 (2013).
12. M. -Y. Hsieh, S.-Y. Kuo, H.-V. Han, J.-F. Yang, Y.-K. Liao, F.-I. Lai, and H.-C. Kuo, "Enhanced broadband and omnidirectional performance of $Cu(In,Ga)Se_2$ solar cells with ZnO functional nanotree arrays," Nanoscale **5**, 3841–3846 (2013).
13. A. Čampa, J. Krč, J. Malmström, M. Edoff, F. Smole, and M. Topič, "The potential of textured front ZnO and flat TCO/metal back contact to improve optical absorption in thin Cu(In,Ga)Se2 solar cells," Thin Solid Films **515**(15), 5968–5972 (2007).
14. Y.-J. Chang and C.-S. Lai, "Toward maximum transmittance into absorption layers in solar cells: investigation of lossy-film-induced mismatches between reflectance and transmittance extrema," Opt. Lett. **38**(17), 3257–3260 (2013).
15. P. J. M. van Laarhoven and E. H. L. Aarts, *Simulated Annealing: Theory and Applications* (Kluwer Academic Publishers, 1987).
16. Z. Qiao, C. Agashe, and D. Mergel, "Dielectric modeling of transmittance spectra of thin ZnO:Al films," Thin Solid Films **496**, 520 – 525 (2006).
17. K. Ellmer, A. Klein, and B. Rech, ed., *Transparent Conductive Zinc Oxide: Basics and Applications in Thin Film Solar Cells* (Springer, 2010).
18. J. Li, J. Chen, M. N. Sestak, C. Thornberry, and R. W. Collins, "Spectroscopic ellipsometry studies of thin film CdTe and CdS: From dielectric functions to solar cell structures," in 34th IEEE Photovoltaic Specialists Conf. pp. 001982–001987 (2009).
19. P. D. Paulson, R. W. Birkmire, and W. N. Shafarmana, "Optical characterization of $CuIn_{1-x}Ga_xSe_2$ alloy thin films by spectroscopic ellipsometry," J. Appl. Phys. **94**(2), 879–888 (2003).
20. E. D. Palik, *Handbook of Optical Constants of Solids* (Academic Press, 1997).
21. D. M. Pozar, *Microwave Engineering* (Addison-Wesley, 1993).
22. P. Yeh, *Optical Waves in Layered Medium* (Wiley, 2005).
23. J. Krč, G. Cernivec, A. Čampa, J. Malmström, M. Edoff, F. Smole, and M. Topič, "Optical and electrical modeling of $Cu(In,Ga)Se_2$ solar cells," Opt. Quantum Electron. **38**(12–14), 1115–1123 (2006).
24. N. G. Dhere, "Toward GW/year of CIGS production within the next decade," Sol. Energy Mater. Sol. Cells **91**, 1376–1382 (2007).

1. Introduction

Urged by increasing demands for reducing the greenhouse gases that are now generally agreed to be the primary cause of global warming, solar energy conversion has gained renewed attention worldwide in the past two decades. Among different photovoltaic cells, the market of thin-film solar cells continues to grow rapidly owing to their strong light absorption property, enabling the reduced material consumption and in turn making the deposition on flexible substrates feasible. Accordingly, thin-film solar modules that are light weight, flexible, low cost, and highly efficient are still very attractive for many applications from consumer electronics to providing electricity in buildings. Copper indium gallium selenide ($CuIn_{1-x}Ga_xSe_2$ or CIGS) is

#200659 - $15.00 USD Received 4 Nov 2013; revised 19 Dec 2013; accepted 25 Dec 2013; published 9 Jan 2014

one of the mainstream thin-film photovoltaic technologies existing nowadays and holds records of the highest efficiency to date among any thin-film solar cell [1, 2].

In the past decade research in thin-film CIGS solar cells for enhancing their quantum efficiency (QE) may largely lean toward the fabrication-/process-oriented studies. Unlike nanostructure-based antireflection (AR) [3–5], discrete multilayer AR coatings [6], and light trapping techniques [7], to name a few, developed for silicon-based solar cells that continue to draw much attention from researchers, only a handful of literature addressed similar issues in CIGS solar cells [8–12]. In [10], three-dimensional studies for AR subwavelength structures (SWSs) with conic, parabolic, and quadratic cross-sectional profiles for different gallium compositions were reported, suggesting that cone-shaped SWSs provide the best transmittance performance. However, the back metal contact was excluded and the conditions for transmittance studies are unclear. On the other hand, QE simulations based on semi-coherent optical model were investigated for hypothetical 100%, 70%, or 20% reflectance from textured ZnO:Al (aluminum-doped zinc oxide, AZO) surface of thin-film CIGS solar cells, indicating that the improvements in QE and short-circuit current originate from the antireflective effect [13]. Studies more closely related to our work presented here may be found in [11], where comparative studies were conducted experimentally for reflection optimizations in kesterite (copper zinc tin selenide, CZTS)/CdS, CIGS/ZnS, and conventional CIGS/CdS devices, all having the same transparent conducting oxide (ZnO and AZO) and a magnesium fluoride (MgF_2) layer.

In spite of all the effort dedicated in improving the QE of CIGS solar cells, most of the work reported so far approach this problem, either experimentally or theoretically, from the reflection point of view. However, as has been reported recently, lossy-film-induced mismatches in layer thickness and incident angle (termed thickness and angular mismatches) between reflectance and transmittance extrema do exist and CIGS solar cells are no exception [14]. Specifically, it has been theoretically shown that in a typical CIGS solar cell the angular mismatch could be at least 10° in about 37% to more than 53% of the spectrum from 350 nm to 1200 nm, depending on the thickness combination of all lossy interlayers [14]. Although using interlayers as a constituent part of the AR coating has been suggested previously (also from the reflection standpoint) without knowing the existence of thickness/angular mismatches [9], it is necessary and of great value to investigate electromagnetically the optimum optical designs (within predefined domains of practical structure variations) of a typical CIGS solar cell for maximizing optical transmittance into the CIGS active layer.

In this paper, we report the optimum interlayers and MgF_2 AR coating designs for a typical CIGS solar cell by suppressing the lossy-film-induced effect from the standpoint of maximum average transmittance into the CIGS absorber. Complex material dispersions of all constituent materials and finite thickness of the CIGS layer with back molybdenum (Mo) contact are all considered in rigorous electromagnetic calculations for broadband (350 nm - 1200 nm) and nearly omnidirectional (0°-80°) incidence. With only a layer of MgF_2 AR coating adopted, which purposely provides the least AR functionality, comparisons are made between optimum designs from minimum average reflectance and maximum average transmittance in terms of their angular and wavelength spectrum behaviors. Finally, the robustness of optimized designs that are obtained under extreme deficiency of angular information but characterized under broadband and nearly omnidirectional incidence is described in detail.

2. Theoretical formulations

The structure considered in this work is schematically illustrated in Fig. 1(a). It consists of a MgF_2 AR coating, the transparent conducting oxide (AZO and ZnO layers) followed by a thin CdS buffer layer for lattice matching to the Mo-backed CIGS active layer. The soda-lime glass on which the cell is generally manufactured was also included in the rigorous electromagnetic

#200659 - $15.00 USD Received 4 Nov 2013; revised 19 Dec 2013; accepted 25 Dec 2013; published 9 Jan 2014

model. The term interlayer used in this work refers to the AZO, ZnO, or CdS layer. For simplicity, all materials, except for ZnO whose birefringence characteristic was taken into account, were assumed non-magnetic, homogeneous, linear, and isotropic.

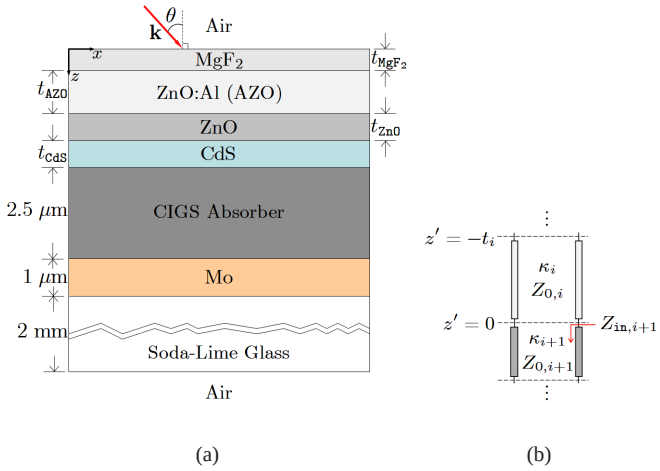

Fig. 1. The structure considered in this work: (a) a typical CIGS solar cell with a MgF_2 AR coating on soda-lime glass and (b) the associated rigorous transmission-line network representation of two adjacent layers within the cell, where $\kappa = \alpha + j\beta$ and Z_0 represent the complex propagation constant and the characteristic impedance, respectively.

To achieve optimum interlayers/AR coating designs, an iterative method combining the simulated-annealing (SA) algorithm and the rigorous transmission-line (TL) network approach [Fig. 1(b)] was applied. Detailed descriptions of the SA algorithm can be found in [15] and it was properly rephrased in the language of a general AR problem in [9]. The algorithm, which is insensitive to the initial values of elements in the parameter vector $\underline{\mathbf{X}}$, attempts to find the global minimum of a cost function $C(\underline{\mathbf{X}})$ that best describes the problem of interest. In the present work, the parameter vector $\underline{\mathbf{X}}$ comprises of the thickness t_i of the MgF_2 layer and all interlayers before the CIGS absorber. Also, complex material dispersions of AZO (2 wt. %) [16], ZnO [17], CdS [18], $CuIn_{1-x}Ga_xSe_2$ with $x = 0.31$ [19], and Mo [20] layers were all taken into account. For simplicity, constant refractive indexes of MgF_2 (1.38233, averaged over ordinary/extraordinary waves and spectral range of interest) and soda-lime glass (1.52833) were adopted. Thus the complex relative permittivity ε_c of each constituent layer was given and the algorithm will be seeking the best thickness combination based on some specific optimization criteria.

2.1. Transmission-line network description of optical transmittance through an arbitrary interface

As the TL-based reflectance calculation for layered medium is well known, we focus ourselves on the transmittance across any interface in multilayered structure in the framework of the TL theory as follows. The essence of connecting the transmittance across each interface with the TL theory is that the transmittance shall always be determined by the incident and net transmitted time-average Poynting vectors that are normal to the interface. When translated to the language of TL theory, they correspond to the input power fed into the line (P_{in}) and the power delivered to the load (P_L), respectively. Consequently, by successively applying the

#200659 - $15.00 USD Received 4 Nov 2013; revised 19 Dec 2013; accepted 25 Dec 2013; published 9 Jan 2014

relation $P_{L,\,i} = P_{\mathrm{in},\,i+1}$ associated with the i-th and $(i+1)$-th layers, the transmittance across any boundary may be obtained.

To proceed without loss of generality, we set $z' = 0$ of a local coordinate system at the $(i+1)$-th interface [Fig. 1(b)]. Then the input power P_{in} at the beginning of the i-th layer, which is t_i above $z' = 0$, is given by $P_{\mathrm{in},\,i}(-t_i) = (1/2)\mathrm{Re}\left[V(-t_i)I^*(-t_i)\right]$ [21], where V and I are the voltage and current waves along the line, respectively, and the asterisk represents the complex conjugate. On the other hand, the power delivered to the load at $z' = 0$ seen by the i-th layer is obtained by simply setting $t_i = 0$ in $P_{\mathrm{in},\,i}(-t_i)$ so that $P_{L,\,i} = P_{\mathrm{in},\,i}(0)$. Since the forward- and backward-propagating voltage and current waves can all be expressed as a function of the forward-propagating voltage amplitude referenced at $z' = 0$ ($V^+_{0,\,i+1}$), the connection between $V^+_{0,\,i+1}$ and $P_{\mathrm{in},\,i}$ is obtained as follows

$$V^+_{0,\,i+1} = \left\{ \frac{2\left(R^2_{0,\,i} + X^2_{0,\,i}\right)^{1/2} P_{\mathrm{in},\,i}}{\left[R_{0,\,i}\left(e^{+2\alpha_i t_i} - |\Gamma_{i+1}|^2 e^{-2\alpha_i t_i}\right) - 2X_{0,\,i}|\Gamma_{i+1}|\sin(\phi_{i+1} - 2\beta_i t_i)\right]} \right\}^{1/2}, \qquad (1)$$

where $\Gamma_{i+1} = (Z_{\mathrm{in},\,i+1} - Z_{0,\,i})\,/\,(Z_{\mathrm{in},\,i+1} + Z_{0,\,i}) = |\Gamma_{i+1}|e^{j\phi_{i+1}}$ denotes the reflection coefficient referenced at the $(i+1)$-th interface (i.e. $z' = 0$), while $Z_{\mathrm{in},\,i+1}$ and $Z_{0,\,i} = R_{0,\,i} + jX_{0,\,i}$ represent the input impedance seen looking downward from the $(i+1)$-th interface and the characteristic impedance of the i-th layer, respectively. The power delivered to the $(i+1)$-th layer or equivalently the transmittance across the $(i+1)$-th interface is then given by

$$P_{\mathrm{in},\,i+1}(z' = 0) = \frac{1}{2}\mathrm{Re}\left[\frac{\left|V^+_{0,\,i+1}\right|^2}{Z^*_{0,\,i}}\left(1 - \Gamma^*_{i+1} + \Gamma_{i+1} - |\Gamma_{i+1}|^2\right)\right] \qquad (2)$$

With $P_{\mathrm{in},\,i}(-t_i)$ and $P_{L,\,i}(0)$ being determined, the absorptance within the i-th layer can simply be written as $A_i = P_{\mathrm{in},\,i}(-t_i) - P_{L,\,i}(0)$.

It should be noted that in arriving at the expression $P_{L,\,i} = P_{\mathrm{in},\,i+1}$, the re-reflection of the reflected wave along the i-th TL line is automatically considered since the voltage wave referenced at the $(i+1)$-th interface is obtained based on the steady-state voltage and current wave solutions prior to interface i. The transmission-line network approach was proved to be computationally efficient when incorporated into the optimization algorithm such as SA in the present work, since the calculations involve no square matrix inverse as described in the 2×2 matrix formulation in [22].

2.2. Descriptions of cost functions in simulated-annealing optimization

To investigate the lossy-film-induced effects on the optical power transmitted into a CIGS solar cell, the cost function used in the SA optimizations may be either the reflectance from the cell's top surface or the transmittance into the CIGS absorber. In either case, the resultant optimized structures were evaluated in terms of the angle-, polarization-, and wavelength-averaged reflectance R_{ave} and transmittance T_{ave} so that further fair comparisons and analyses can be made accordingly.

When the average reflectance minimum is pursued, the corresponding cost function $C_R(\underline{\mathbf{X}})$ is defined as

$$C_R(\underline{\mathbf{X}}) = \frac{\int_{\Delta\theta}\int_{\Delta\lambda}\left[|\Gamma_{\mathrm{TE}}(\underline{\mathbf{X}},\lambda,\theta)|^2 + |\Gamma_{\mathrm{TM}}(\underline{\mathbf{X}},\lambda,\theta)|^2\right] I(\lambda)\,d\lambda\,d\theta}{2\int_{\Delta\theta}\int_{\Delta\lambda} I(\lambda)\,d\lambda\,d\theta}, \qquad (3)$$

#200659 - $15.00 USD Received 4 Nov 2013; revised 19 Dec 2013; accepted 25 Dec 2013; published 9 Jan 2014

where $|\Gamma_{\mathrm{TE}}(\underline{\mathbf{X}},\lambda,\theta)|^2$ and $|\Gamma_{\mathrm{TM}}(\underline{\mathbf{X}},\lambda,\theta)|^2$ are the reflectance associated with TE and TM polarization, respectively, and $I(\lambda)$ represents the solar spectrum irradiance. Note that if the solar spectrum weighting (SSW) is not considered, the definition of the cost function is still valid for $I(\lambda)=1$.

On the contrary, to maximize the average transmittance into the CIGS active layer, the associated cost function has to be modified as given below:

$$C_T(\underline{\mathbf{X}}) = 1 - \frac{\int_{\Delta\theta}\int_{\Delta\lambda}[T_{\mathrm{TE}}(\underline{\mathbf{X}},\lambda,\theta)+T_{\mathrm{TM}}(\underline{\mathbf{X}},\lambda,\theta)]I(\lambda)d\lambda d\theta}{2\int_{\Delta\theta}\int_{\Delta\lambda}I(\lambda)d\lambda d\theta}, \tag{4}$$

where $T_i(\underline{\mathbf{X}},\lambda,\theta)$, $i=\{\mathrm{TE},\mathrm{TM}\}$, denotes the transmittance into the CIGS absorber. Given the $C_T(\underline{\mathbf{X}})$ above, the parameter vector $\underline{\mathbf{X}}$ leading to a maximum average transmittance will be pursued as the SA algorithm seeks the global minimum of any cost function.

3. Results and discussions

The results presented hereafter correspond to structurally-uniform CIGS solar cells with one-layer MgF_2 AR coating. The cell itself composed of ZnO:Al (AZO, 2 wt.%)/ZnO/CdS stack followed by a 2.5-μm-thick CIGS absorption layer, 1 μm-thick Mo back contact, and a soda-lime glass of 2 mm in thickness [Fig. 1(a)]. To make this research more practically valuable, the domains of variables of $C_i(\underline{\mathbf{X}})$, $i=\{R,T\}$ were strictly confined within ranges close to typical values reported in the literature [23, 24], as summarized in Table 1.

Table 1. Domains of Variables of the Cost Function $C_i(\underline{\mathbf{X}})$, $i=\{R,\ T\}$, Used in Simulated-Annealing Optimizations.

Parameter	Lower Limit	Upper Limit	Unit
MgF_2 Thickness, $t_{\mathtt{MgF_2}}$	90	500	nm
AZO Thickness, $t_{\mathtt{AZO}}$	150	1000	nm
ZnO Thickness, $t_{\mathtt{ZnO}}$	40	90	nm
CdS Thickness, $t_{\mathtt{CdS}}$	40	100	nm

3.1. SA optimizations based on criteria of minimum average reflectance and maximum average transmittance

Table 2 lists the performance comparisons between SA-optimized MgF_2 AR coating and interlayer thicknesses obtained based on criteria of minimum average reflectance [$C_R(\underline{\mathbf{X}})$, Eq. (3)] and maximum average transmittance [$C_T(\underline{\mathbf{X}})$, Eq. (4)], all in the absence of solar spectrum weighting. Both R_{ave} and T_{ave} were averaged over TE and TM polarization, angle of incidence $\theta=[0^\circ,80^\circ]$, and the wavelength spectrum $\lambda=[350,1200]$ nm. As clearly indicated, the difference in the $C_T(\underline{\mathbf{X}})$- and $C_R(\underline{\mathbf{X}})$-based average reflectance R_{ave} is merely 0.3%; however, the average transmittance T_{ave} associated with $C_T(\underline{\mathbf{X}})$-based structure is larger by 14.34% than its $C_R(\underline{\mathbf{X}})$-based counterpart.

To better visualize the distinct results reported in Table 2, in particular the average transmittance, the polarization-averaged reflectance $R(\lambda,\theta)$ and transmittance $T(\lambda,\theta)$ plots calculated for the structures given in Table 2 are shown in Figs. 2 and 3, respectively. The reflectance

#200659 - $15.00 USD Received 4 Nov 2013; revised 19 Dec 2013; accepted 25 Dec 2013; published 9 Jan 2014

Table 2. Performance and Layer Thickness (in nm) Comparisons between SA-Optimized Results Based on Minimum Average Reflectance [$C_R(\underline{\mathbf{X}})$, Eq. (3)] and Maximum Average Transmittance [$C_T(\underline{\mathbf{X}})$, Eq. (4)] Criteria, All without Solar Spectrum Weighting (SSW), for a Typical CIGS Solar Cell.

Cost Function w/o SSW	R_{ave} (%)	T_{ave} (%)	$t_{\mathrm{MgF_2}}$	t_{AZO}	t_{ZnO}	t_{CdS}
Min. Ave. Reflectance, $C_R(\underline{\mathbf{X}})$	5.88	66.71	110.11	966.57	69.78	49.06
Max. Ave. Transmittance, $C_T(\underline{\mathbf{X}})$	6.18	81.05	117.88	150.00	89.97	40.00

*R_{ave} and T_{ave} were averaged over TE and TM polarization, $\lambda = [350, 1200]$ nm, and $\theta = [0^\circ, 80^\circ]$.

figures look alike at the first glance, except that $C_R(\underline{\mathbf{X}})$-based $R(\lambda,\theta)$ exhibits fast-varying ripple-like behaviors, in particular at shorter wavelengths. This may be attributed to strong superpositions of transmitted and reflected waves existing within a much thicker AZO layer that is several times larger than the wavelength in the medium. On the contrary, significant differences in $T(\lambda,\theta)$ figures are revealed in that the maximum transmittance criterion not only significantly extends the high-$T(\lambda,\theta)$ spectral range to longer wavelengths, but notably improves the $T(\lambda,\theta)$ level over most of the spectrum of interest.

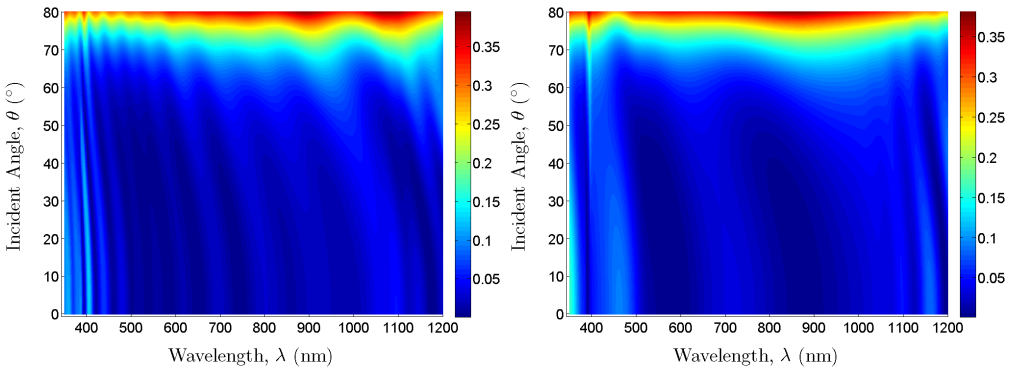

(a) (b)

Fig. 2. Polarization-averaged reflectance $R(\lambda,\theta)$ obtained based on criteria of minimum average reflectance (a) and maximum average transmittance (b) for a typical CIGS solar cell.

Another way to quantify in a more precise manner the differences between $C_T(\underline{\mathbf{X}})$- and $C_R(\underline{\mathbf{X}})$-based results may be illustrating the angle-averaged reflectance $R_{\theta-ave}$ and transmittance $T_{\theta-ave}$ with varying wavelength, as given in Fig. 4. With the presence of a MgF_2 AR coating and the absence of SSW, the $C_R(\underline{\mathbf{X}})$-based angle-averaged reflectance behaves slightly better than its $C_T(\underline{\mathbf{X}})$-based counterpart for $\lambda \approx [391, 734]$ nm [the largest red region in Fig. 4(a)]. On the other hand, the maximum average transmittance criterion enhances $T_{\theta-ave}$ at all wavelengths within the spectrum of interest, with the improvement of $> 5\%$ for wavelengths

#200659 - $15.00 USD Received 4 Nov 2013; revised 19 Dec 2013; accepted 25 Dec 2013; published 9 Jan 2014

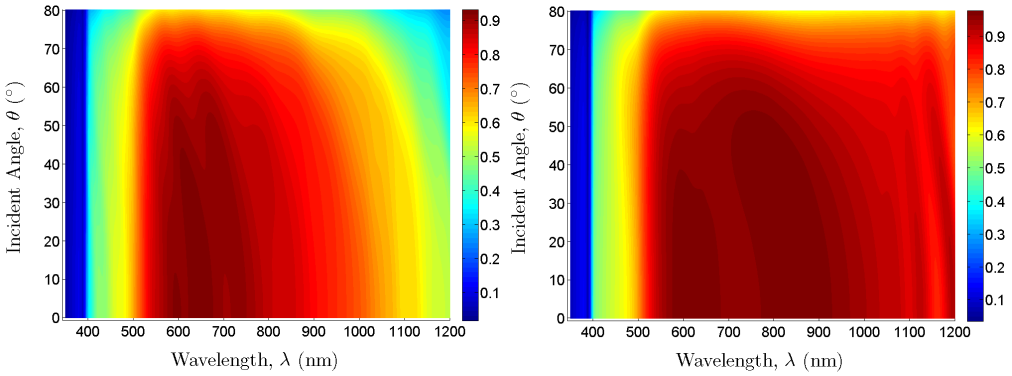

(a) (b)

Fig. 3. Polarization-averaged transmittance $T(\lambda,\theta)$ obtained based on criteria of minimum average reflectance (a) and maximum average transmittance (b) for a typical CIGS solar cell.

beyond 661 nm and $>10\%$ for $\lambda > 776.5$ nm.

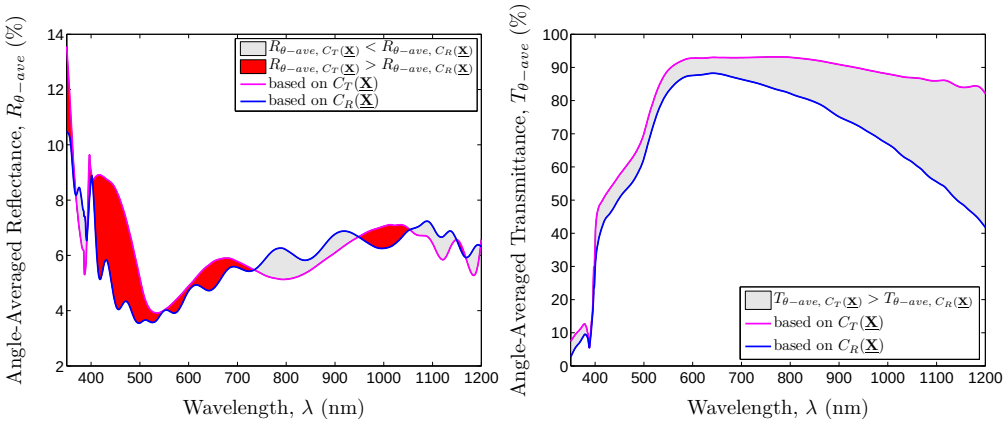

(a) (b)

Fig. 4. Comparisons between the angle-averaged reflectance (a) and transmittance (b) associated with SA-optimized MgF_2/interlayer thicknesses based on minimum average reflectance $C_R(\underline{\mathbf{X}})$ and maximum average transmittance $C_T(\underline{\mathbf{X}})$ criteria.

3.2. Transmittance enhancement by suppressing lossy-film-induced angular mismatches

The remarkable difference in T_{ave} across CdS-CIGS interface apparently results, to a large extent, from the difference in the AZO thickness. It is minimized to just 150 nm, the lower limit of t_{AZO} searching range (see Table 1), if achieving a maximum average transmittance is preferred. On the contrary, the AZO thickness is increased up close to the allowed upper limit

#200659 - $15.00 USD Received 4 Nov 2013; revised 19 Dec 2013; accepted 25 Dec 2013; published 9 Jan 2014

(1000 nm [24]) when reaching the average reflectance minimum is required. The results are consistent with the findings reported in [14] where a thicker lossy film would generally lead to a smaller reflectance.

However, the significant enhancement in T_{ave} cannot be fully explained by a large reduction in AZO thickness. In fact, the ZnO thickness is increased by 28.93%, suggesting that the T_{ave} optimization may not be achieved simply by decreasing the thickness of all lossy interlayers. To further physically explain the reasons behind the differences between $C_T(\underline{\mathbf{X}})$- and $C_R(\underline{\mathbf{X}})$-based results, Fig. 5 shows the wavelength-dependent angular mismatch associated with the optimized structures given in Table 2. Note that the angular mismatch at each wavelength is the difference in the incident angles at which the polarization-averaged $R(\lambda,\theta)$ and $T(\lambda,\theta)$ extrema occur in a fixed structure. As seen in Fig. 5(b), the angular mismatch is greatly suppressed with the $C_T(\underline{\mathbf{X}})$-based structure when compared with the $C_R(\underline{\mathbf{X}})$-based counterpart [Fig. 5(a)].

As a comparison, Fig. 5(c) shows the angular mismatch spectrum associated with a CIGS solar cell having the interlayer thicknesses be at their respective minima $[(t_{\mathtt{AZO}}, t_{\mathtt{ZnO}}, t_{\mathtt{CdS}}) = (150, 40, 40)$ nm](Table 1). The interlayer thickness was such chosen so that the ZnO thickness is the only difference between the $C_T(\underline{\mathbf{X}})$-based structure and the one considered in Fig. 5(c). We see that the cell with minimum interlayer thicknesses, although exhibits smaller mismatch peaks, does suffer a wider spectral range having an angular mismatch of $> 5^\circ$ when compared with that in Fig. 5(b). Further investigations show that even when the MgF_2 layer is optimized for the cell with minimum interlayer thicknesses, its average transmittance is still limited to 80.32%, which is 0.73% shy of the best case in Table 2. It then follows that the significant enhancement in the average transmittance may be fully attributed to the global suppression of angular mismatches over the entire CIGS absorption spectrum.

3.3. Robustness studies of SA-optimized designs

Following the investigations described above that are mainly based upon broadband and omnidirectional considerations, a natural question may arise: What is the difference between $C_R(\underline{\mathbf{X}})$- and $C_T(\underline{\mathbf{X}})$-based results obtained under normal incidence only? To address this question, the optimizations were conducted with identical settings mentioned above, except for a fixed incident angle at 0°. The results are shown in Table 3. Note that the R_{ave} and T_{ave} in the table were, again, calculated over the spectral and angular ranges of $\lambda = [350, 1200]$ nm and $\theta = [0^\circ, 80^\circ]$, respectively, despite that the structure parameters were optimized at $\theta = 0^\circ$ only. It is interesting to learn that the $C_T(\underline{\mathbf{X}})$-based R_{ave} and T_{ave} all outperform their $C_R(\underline{\mathbf{X}})$-based counterparts.

On the other hand, it is also worth mentioning that, when characterized at $\theta = 0^\circ$, the $C_R(\underline{\mathbf{X}})$-based case in Table 3 exhibits respective average reflectance R'_{ave} and transmittance T'_{ave} (averaged over the polarization states and wavelengths) of 1.98% and 79.87%, while those for the $C_T(\underline{\mathbf{X}})$-based one are 2.61% and 84.67%, respectively. Hence there is no surprise that, when properly optimized, both $C_R(\underline{\mathbf{X}})$- and $C_T(\underline{\mathbf{X}})$-based structures have their own advantage in either R'_{ave} or T'_{ave} as expected. However, it is when characterizing them under broadband and nearly omnidirectional conditions that differentiates their performance in a more practical manner. Also, comparing with the results shown in Table 2, we see that, although the $C_R(\underline{\mathbf{X}})$-based T_{ave} is increased significantly, the $C_T(\underline{\mathbf{X}})$-based R_{ave} and T_{ave} values are hardly changed. This may suggest that the maximum average transmittance criterion could be more robust to the deficiency of angular information during the optimization process.

The potential robustness mentioned above may be best justified by considering the average reflectance and transmittance as a function of the incident angle at which the structure is actually optimized. The results are shown in Fig. 6, where two sets of results obtained from $C_R(\underline{\mathbf{X}})$- and $C_T(\underline{\mathbf{X}})$-based optimizations are given. Note that each marker in the figure corresponds to one structure optimized at the corresponding incident angle in the figure. It is surprising to learn

#200659 - $15.00 USD Received 4 Nov 2013; revised 19 Dec 2013; accepted 25 Dec 2013; published 9 Jan 2014

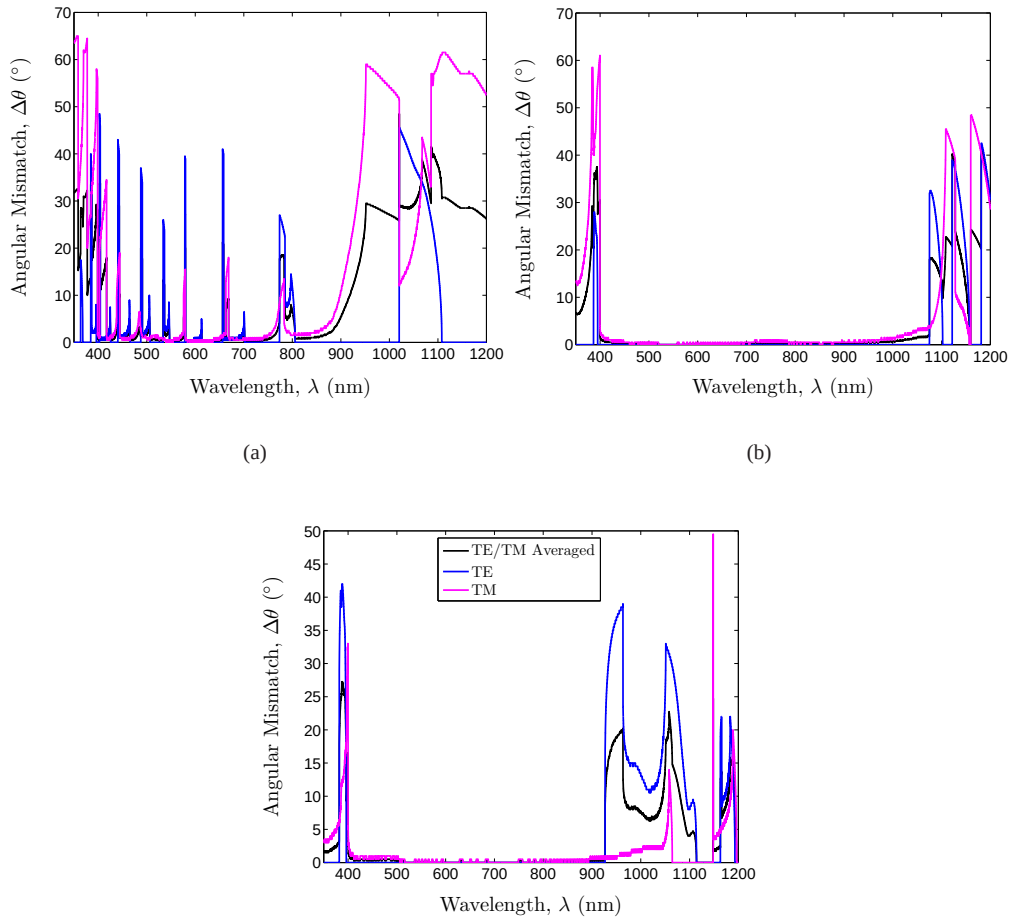

Fig. 5. Comparisons in angular mismatch spectra among some CIGS solar cell designs: (a) based on minimum average reflectance, $C_R(\underline{\mathbf{X}})$, (b) based on maximum average transmittance, $C_T(\underline{\mathbf{X}})$, and (c) by setting the interlayer thicknesses to their respective minima $[(t_{\mathtt{AZO}}, t_{\mathtt{ZnO}}, t_{\mathtt{CdS}}) = (150, 40, 40)$ nm].

#200659 - $15.00 USD Received 4 Nov 2013; revised 19 Dec 2013; accepted 25 Dec 2013; published 9 Jan 2014

Table 3. Performance and Layer Thickness (in nm) Comparisons between SA-Optimized Results Obtained Based on Minimum Average Reflectance [$C_R(\underline{\mathbf{X}})$, Eq. (3)] and Maximum Average Transmittance [$C_T(\underline{\mathbf{X}})$, Eq. (4)] Criteria, All without Solar Spectrum Weighting (SSW), for a Typical CIGS Solar Cell under Normal Incidence.

Cost Function w/o SSW	R_{ave} (%)	T_{ave} (%)	t_{MgF_2}	t_{AZO}	t_{ZnO}	t_{CdS}
Min. Ave. Reflectance, $C_R(\underline{\mathbf{X}})$	6.31	75.04	94.07	416.75	64.20	47.28
Max. Ave. Transmittance, $C_T(\underline{\mathbf{X}})$	6.07	80.90	100.72	150.00	90.00	40.02

*R_{ave} and T_{ave} were averaged over TE and TM polarization, $\lambda = [350, 1200]$ nm, and $\theta = [0°, 80°]$.

that $C_T(\underline{\mathbf{X}})$-based R_{ave} surpasses those from $C_R(\underline{\mathbf{X}})$-based optimizations for $\theta < 30°$. It is only at larger incident angles ($\theta > 30°$, approximately) will $C_R(\underline{\mathbf{X}})$-based optimizations become more effective in minimizing the average reflectance. Moreover, when optimized at a single incident angle with minimum R_{ave} consideration, the structure having the best R_{ave} performance is the one synthesized at $\theta = 45°$, rather than at $\theta = 0°$, since the 45°-optimized design can easily compensate angle of incidence toward 0° and 90°, averaging out elevation variations in omnidirectional incidence.

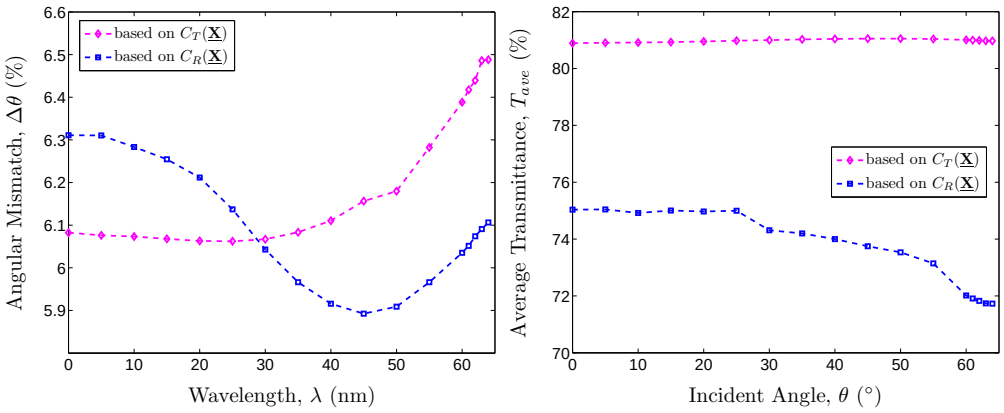

(a) (b)

Fig. 6. Robustness studies of the structure to broadband and nearly-omnidirectional incidence when it was optimized at a single incident angle based on cost function $C_T(\underline{\mathbf{X}})$ or $C_R(\underline{\mathbf{X}})$: (a) the average reflectance R_{ave}, and (b) the average transmittance T_{ave}. Quantities R_{ave} and T_{ave} were averaged over the TE/TM, $\lambda = [350, 1200]$ nm, and $\theta = [0°, 80°]$. The horizontal axis represents the incident angle at which the optimization is conducted.

On the contrary, and perhaps more important findings are revealed in Fig. 6(b). While the $C_R(\underline{\mathbf{X}})$-based T_{ave} decreases when θ is beyond 25°, the $C_T(\underline{\mathbf{X}})$-based T_{ave} is highly insensitive to the incident angle at which the structure is optimized. The difference between the two T_{ave} curves is constantly larger than 5%. In fact, even being optimized at a single incident angle, the

#200659 - $15.00 USD Received 4 Nov 2013; revised 19 Dec 2013; accepted 25 Dec 2013; published 9 Jan 2014

thickness of all interlayers associate with $C_T(\underline{\mathbf{X}})$-based structure is nearly identical to that given in Table 2 (obtained from nearly omnidirectional incidence). The MgF_2 thickness appears to be the only major difference among all the optimized structures, which is increased with the incident angle for maintaining the impedance seen looking downward from the top surface. This indicates that, with the adoption of maximum average transmittance criterion, the MgF_2 AR coating and interlayer thicknesses may be optimized at any single incident angle within the range of $\theta = [0^\circ, 65^\circ)$, which can largely reduce the required computational resources without compromising the optical transmittance into the CIGS active layer.

4. Summary

The investigation of optimum optical designs of interlayers and a MgF_2 AR coating for maximum average transmittance (T_{ave}) into the CIGS absorber of a typical CIGS solar cell by suppressing lossy-film-induced angular mismatches has been described. Simulated-annealing algorithm incorporated transmission-line theory tailored to this problem enables rigorous (without approximation) yet fast optimizations, in particular for the transmittance across any interface within the cell. The cell with a MgF_2 AR coating and optimized based on the criterion of maximum T_{ave} into the CIGS absorber is shown to achieve an optimum T_{ave} of $> 81\%$ (over $\lambda = [350, 1200]$ nm and $\theta = [0^\circ, 80^\circ]$ on $t_{\mathtt{CIGS}} = 2.5\ \mu$m) and an average reflectance (R_{ave}) of 6.18%. However, when a minimum R_{ave} is pursued, the optimized cell structure (also with a MgF_2 AR coating) exhibits 5.88% R_{ave} but suffers a significant loss in T_{ave} (which is only 66.71%) due to a much thicker transparent conductive oxide layer for achieving low reflectance at large incident angles.

Further investigations show that the maximum T_{ave} criterion enhances the angle-averaged transmittance $T_{\theta-ave}$ over the whole spectrum of interest, with the improvement of $> 5\%$ for wavelengths beyond 661 nm and $> 10\%$ for $\lambda > 776.5$ nm. Also, the T_{ave} enhancement is shown to be achieved perhaps only by suppressing globally the lossy-film-induced angular mismatches over the whole CIGS absorption spectrum. Decreasing all interlayer thicknesses to their respective minima, though largely improves T_{ave}, may not necessarily result in the optimum design in terms of broadband angular mismatch suppression and the highest T_{ave} into the CIGS active layer.

Suppressing the lossy-film-induced mismatches through the maximum T_{ave} criterion, which treats the AR coating and all interlayers as a whole, can lead to optimized cell structures that are more robust to broadband and omnidirectional incidence. The results show that, even optimized at a single incident angle but characterized over broadband and nearly omnidirectional incidence, each optimized structure has a nearly identical T_{ave} performance, all larger than 80%. This research may thus provide the theoretical background and design principles for simple, low-cost, yet highly efficient CIGS solar cells and for some other optical/photonic devices with lossy films in the optical path.

#200659 - $15.00 USD Received 4 Nov 2013; revised 19 Dec 2013; accepted 25 Dec 2013; published 9 Jan 2014